LAWRENCE
LIVERMORE
NATIONAL
LABORATORY

UCRL-TR-227391

Detection and Attribution of Regional Climate Change

G. Bala, A. Mirin

January 22, 2007

Disclaimer

This work performed under the auspices of the U.S. Department of Energy by Lawrence Livermore National Laboratory under Contract DE-AC52-07NA27344.

FY06 LDRD Final Report
Detection and Attribution of Regional Climate Change
LDRD Project Tracking Code: 05-ERD-042
Govindasamy Bala, Principal Investigator

Abstract

We developed a high resolution global coupled modeling capability to perform breakthrough studies of the regional climate change. The atmospheric component in our simulation uses a 1^o lat x1.25^o lon -grid which is the finest resolution ever used for the NCAR coupled climate model CCSM3. Substantial testing and slight retuning was required to get an acceptable control simulation. The major accomplishment is the validation of this new high resolution configuration of CCSM3. There are major improvements in our simulation of the surface wind stress and sea ice thickness distribution in the Arctic. Surface wind stress and ocean circulation in the Antarctic Circumpolar Current are also improved. Our results demonstrate that the FV version of the CCSM coupled model is a state of the art climate model whose simulation capabilities are in the class of those used for IPCC assessments. We have also provided 1000 years of model data to Scripps Institution of Oceanography to estimate the natural variability of stream flow in California. In the future, our global model simulations will provide boundary data to high-resolution mesoscale model that will be used at LLNL. The mesoscale model would dynamically downscale the GCM climate to regional scale on climate time scales.

1. Introduction/Background

We can infer from observational and global climate modeling studies that increasing levels of greenhouse gases will over decadal time scales produce climate change that greatly exceeds rates of change during the past few hundred thousand years. Detection and attribution of climate change to human causes requires that we demonstrate that the observed changes cannot be accounted for by the natural variability of the climate system. A key goal of the climate research community is to detect and attribute climate change, using a combination of observations and numerical modeling of the climate system.

Detection and attribution of climate change has primarily been based on the statistical analysis of global scale quantities such as near surface temperatures, satellite based temperature measurements, height of the tropopause, ocean heat content, sea ice extent, length of the growing season, sea level pressure etc. Much progress has been made using these global scale quantities; the weight of evidence now points to significant human impact on climate during the twentieth century. The Intergovernmental Panel on Climate Change (IPCC) concluded in 2001 that “There is new and stronger evidence that most of the warming observed over the last 50 years is attributable to human activities”.

In summary, the detection of climate change typically involves:

- Developing statistical methodologies capable of detecting climate change
- Long climate model runs without changing external human forcing in order to estimate the internal climate variability
- Long unbiased records of climate variables, or their proxies, that can be used to estimate natural climate variability
- Establishing statistical significance of trends by comparison of observed changes to natural variability

The attribution of climate change requires:

- Estimates of the anthropogenic forcing of climate, e.g. fluxes of greenhouse gases, aerosols, land use change
- Incorporation of anthropogenic forcing in climate models
- Long climate model runs including anthropogenic and natural forcing e.g. the climate of the 20th century
- Quantitative comparison of observed climate signals with expected signatures of human activities

The detection and attribution of climate change at the global scale provides essential confirmation of the effects of human activities on climate. However, global-scale detection and attribution provides very limited information regarding regional scale changes. Policy decisions concerning the adaptation and response to climate change need to be made at the regional to local scales. Hence the focus of the proposed research is to develop the capability to detect and attribute climate change at regional scales. Figure. 1 indicates that GCMs and observation-based data sets can achieve a level of agreement sufficient for climate detection and attribution.

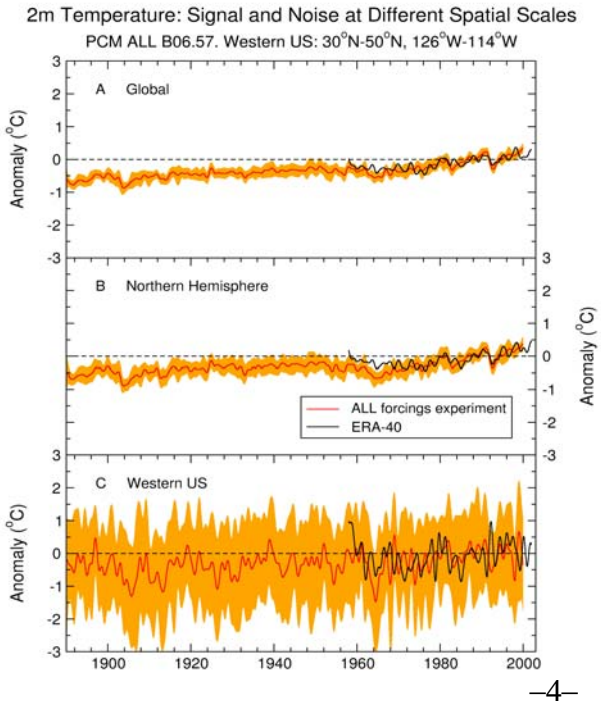

Figure 1: The signal and variability (noise) in 2m air temperatures at a range of spatial scales. The shaded region is the between realization variability in the PCM ensemble runs. At the scale of the western US this variability becomes much larger when compared to the global and hemispheric averages. However, surface temperature changes in DOE-Parallel Climate Model (PCM) and ERA-40 (a reanalysis product incorporating available observational data) show consistency even at sub-global spatial scales. This result demonstrates that regional climate detection and attribution is a both a challenging and a promising area of research.

This Exploratory Research project, titled Detection and Attribution of Regional Climate Change", is a two-year effort to establish the modeling framework for studying regional climate in California. The main goal is detect regional climate change in hydrological variables such as stream flow and snow depth. As an end product of this 2-year effort, we now have a capability in high resolution coupled climate capability that is the best in the nation. Through this effort we insure that this capability is exploited and improved to keep us at the forefront in the regional climate modeling studies. In the future, our global model simulations will provide boundary data to high-resolution mesoscale model that will be used at LLNL.

This report consists of several parts. In section 2 we describe the computational model. We then discuss two scientific experiments: In section 3, we discuss a long pre-industrial control simulation, and in section 4 we discuss the validation of a long present-day control simulation. In section 5 we discuss model improvements for future simulations. The exit plan is given in section 6. A summary is presented in Section 7, and the references are given in Section 8.

2. Computational Model

The global coupled model is NCAR Community Climate System Model version 3 (CCSM3). It has the following sub-model components: The Community Atmosphere Model version 3 (CAM3; Collins, W. D. et al. 2006), the Community Land Surface Model version 3 (CLM3; Dickinson et al. 2006), the Community Sea Ice Model version 5 (CSIM5; Briegleb et al. 2004), and Parallel Ocean Model version 1.4.3 (POP; Smith and Gent 2004). CCSM3 has been designed to produce simulations with reasonable fidelity over a wide range of resolutions and with a wide variety of atmospheric dynamical frameworks (Hack et al. 2006;Rasch et al. 2006;Yeager et al. 2006).

For the simulations presented here, we use the Finite Volume (FV) dynamical core for the atmospheric component. The horizontal resolution is 1 degree in latitude and 1.25 degree in longitude. Hereafter, this configuration will be referred to as FVx1. There are 60 % more grid points in this configuration than T85. This change in the configuration necessitated slight retuning of the model. The tuning procedure involved changes to parameters in the cloud and convection parametrizations within an acceptable range (Table 1). The tuning is performed on the uncoupled atmosphere model CAM3 using prescribed observed climatological sea surface temperatures and sea ice. In this iterative tuning procedure, we attempt to bring the meridional distribution of the zonal-mean shortwave and longwave cloud radiative forcing into reasonable agreement with ERBE (Barkstrom and Smith 1986) observations. The global- and annual-mean net energy flux at the top of the atmosphere is also reduced to within a few tenths of a W m^{-2}.

Initial tests using this tuned model showed that excessive marginal sea ice was simulated in the Arctic in the Davis Strait off Greenland during the winter. The main cause was that

the amplitude of seasonal cycle in the Arctic sea ice concentration was unrealistically larger than the observed amplitude. In order to correct this bias, we turned off the nonlinear Smagorinsky viscosity option in the anisotropic formulation of horizontal diffusion for momentum components in the ocean model (Smith and Gent 2004). Instead, we adopted the linear option wherein the viscous tensor is linearly related to the velocity gradients. The Smagorinsky viscosity tends to damp the currents strongly near curved coastlines, and thus it weaks the west Greenland current into the Davis Strait significantly (Peter Gent, personal communication), leading to excessive sea ice in the Ladrador Sea. A detailed analysis of the sensitivity of the simulated climate to the choice of the viscosity formulation is beyond the scope of this paper. All other aspects of the model are similar to the T85 configuration discussed by (Collins, W. D. et al. 2006).

3. 1000-yr pre-industrial control simulation

We performed a stable1000-yr long pre-industrial control simulation for the purpose of evaluating the noise in hydrological variables. The stability of the long control simulation can be seen from Fig. 2. The illustration demonstrates that the total variability as measured by standard deviation in modeled surface temperature increases as the spatial domain decreases. Similar characteristic of variability is also noted in other variables such as precipitation. The simulation shows very small drift; we measured the drift as 0.05 K per century.

We provided the climate data to UCSD via high-speed transfer to San Diego Supercomputing Center. The collaborators at UCSD use this data for the regional detection and attribution study. The climate model output is first statistically downscaled to provide regional information over California. The statistical downscaling is performed at UC San Diego. The downscaled climate is then used to drive a hydrology model to obtain runoff and other important hydrological variables.

4. 400-yr present-day control simulation

The FVx1 configuration is validated in the section. We performed the FVx1 simulation for 400 years, starting from the observed ocean (Levitus et al. 1998) and sea ice data. This simulation is a present-day control simulation using greenhouse concentrations for CO_2, CH_4, N_2O, CFC-11, and CFC-12 prescribed at year 1990 levels of 355 ppmv, 1714 ppbv, 311 ppbv, 280 pptv, and 503 pptv, respectively. In this paper, this simulation is compared to a corresponding 700-year T85 present-day control simulation performed at NCAR. Although we have made a thorough analysis of the simulation, only comparisons of a few key variables are presented in this report.

4.1 Global mean climate

Global- and annual-means along with root mean square errors of selected climate variables (Table 2) show that the global mean FVx1 climate is nearly identical to T85 climate. The global- and annual-mean shortwave and longwave cloud forcings are reproduced in both T85 and FVx1 to match the ERBE estimates (Barkstrom and Smith

1986) to within 0.1 Wm^{-2}. The physical parameterizations are unchanged from T85 to FVx1, and our retuning of the tunable cloud parameters in FVx1 was responsible for this match with observations. The model differences are less than 1 Wm^{-2}. The root mean square errors in circulation related quantities such as sea level pressure, 200-mb zonal wind and 500-mb geopotential are slightly reduced in FVx1, suggesting marginal improvement in the atmospheric circulation.

4.2 Sea surface temperature

In general, both T85 and FVx1 generate equatorial surface water in the eastern Pacific that is colder than observed (HadISST dataset; Rayner et al. 2003) which extends too far west into the warm pool (Fig. 3). However, significant improvements can be seen in narrow coastal regions near Peru, Chile, and Baja, California. Cold SST biases in the North Atlantic are also significantly reduced in FVx1. However, off the coast of Brazil, the cold biases are increased. The North Pacific is warmer in FVx1 so that the cold bias in the western part of the basin is replaced by a smaller warm bias, and the warm bias in the eastern part of the basin is enhanced. The RMS error over the global domain is reduced from 1.54 K in T85 to 1.42 K in FVx1, indicating marginal improvement. The correlation between the two SST error patterns shown in Fig. 3 is 0.83, indicating strong similarity in the SST simulated by the two versions of the model.

4.3 Surface wind stress

By many measures, the simulation of surface wind stress in FVx1 shows improvement over T85 (Fig. 4) when are compared to ERS (Queffeulou et al. 1999) satellite observations . The mean RMS error decreases from 0.037 Nm^{-2} to 0.032 Nm^{-2} in FVx1. The overestimation of the wind stress in the North Pacific and the Gulf Stream region of the North Atlantic in T85 are reduced in FVx1. The improved simulation of SST (Fig. 3) is associated with an improved wind stress simulation (Fig. 4) in these regions. There is also some reduction in the wind stress bias in the Antarctic Circumpolar Current region. The Southern Hemisphere storm track region is shifted to the south in FVx1, in better agreement with observations; similar improvement was noticed when the spectral model resolution was increased from T42 to T85 (Hack et al. 2006). The correlation between the two error patterns shown in Fig. 2 for the magnitude of wind stress is 0.89, indicating strong similarity of the two model versions.

4.4 Sea ice thickness

The mean sea ice thickness in the central Arctic is about 2 to 2.5 meters in both the simulations (Fig. 5), in reasonable agreement with submarine measurements of sea ice thickness (Rothrock et al. 1999). The regional distribution has improved in the FV x 1 simulation relative to the T85 simulation, notably in the Canadian Archipelago and East Siberian Sea. The T85 simulation underestimates the sea ice in the Canadian Archipelago by 1 meter and overestimates by 2 meters in the East Siberian Sea (Collins, W. D. et al. 2006). This bias has been reduced by 0.6 meters or more in the FVx1

simulation. The sea ice thickness is about 4 to 5 meters in the Canadian Archipelago, in good agreement with observations.

4.5 Comparison to other IPCC models

We compare the CCSM3 FVx1 and T85 simulations to present-day control simulations available from the CMIP3 (Coupled Model Intercomparison Project 3) database (http://www-pcmdi.llnl.gov/ipcc/about_ipcc.php). The CMIP3 simulations are from the following models: PCM, MIUB-ECHO-G, MRI-CGCM2.3.2a, and UKMO-HadCM3, each with documentation available at the CMIP3 website. For each model, 20 year climatologies were computed for selected variables, and global scale statistics were computed comparing the simulations with available reference datasets. We display these statistics on Taylor diagrams (Taylor 2001), which portrays the standard deviation, correlation and the centered RMS on a single diagram. In Fig. 6, colors identify variables and small circles indicate the models other than the T85 and FVx1 simulations in the CMIP3 database.

Space-time statistics over the annual cycle and global domain are shown in Fig.6a. For each variable, Fig.6a shows that the range of errors among all models is much greater than the difference in error between FVx1 and T85. For both the T85 and FVx1 runs the variance is too large in the zonal wind stress, 850hPa winds and sea level pressure, but similar problems can be identified in all models. Annual cycle space-time statistics for the tropics (20S-20N) are shown in Fig.6b. The annual cycle is generally weaker in the tropics, and the correlation and RMS are therefore more heavily influenced by the spatial characteristics of the fields. Surface air temperature and geopotential are quite smooth, and not strongly constrained by the insolation pattern, so their correlations are consequently lower than in Fig 6a.

Fig.6c is analogous to Fig.6a, b, with the domain limited to the Northern Hemisphere extratropics (20N-90N) and with the zonal mean for each calendar month removed before the statistics are computed. This highlights characteristics associated with stationary wave patterns induced by land-sea contrasts or orography (e.g., the Rockies). While the correlations are generally lower than in Fig.6a, for most fields the scatter is smaller among models, presumably because of the additional geographical constraints. The overall impression conveyed by Fig.6 is that the magnitude of errors in the FVx1 and T85 model simulations are nearly the same and generally no larger or smaller than other coupled climate models.

5. Model Improvements for Future Studies

In addition to the major biases such as the double ITCZ, and the 2-year periodicity of the ENSO cycle, we find that the other troublesome model biases persist in our high resolution simulation such as: the colder tropopause in the high latitudes, warmer winter time land temperature in the high latitudes, precipitation deficits in the southeast United States, Amazonia, and the Southeast Asia, warmer SST in the western coastal regions, the semiannual SST cycle in the eastern Pacific, and the underestimation of downwelling

solar radiation in Arctic. We are presently investigating how these biases could be reduced.

This study used the NCAR CCSM3 at about 1 degree resolution. Our aim is to increase the resolution of both the atmosphere and ocean models in the future. Increased resolution of the atmosphere will enable us to better represent physical processes at the regional scale. We intend to increase the resolution of the atmospheric model progressively to one quarter of a degree. At this resolution, the entire global domain has a resolution of the state-of-the-art mesoscale models. The main bottlenecks for simulations of this kind are computational resources such as CPU time and storage. For the coupled configuration, the ocean model resolution should be finer than the atmosphere model. We aim to increase the resolution of the ocean model to one tenth of a degree with help from our collaborators at Scripps Institution of Oceanography. Concurrently, we are also working on developing a mesoscale modeling capability at LLNL. The mesoscale model will be run at about a 10 km resolution in a climate model.

6. Exit Plan and Return to Laboratory

The work discussed here is part of the E&E directorate's overall strategic plans for future program development in the area of regional climate modeling. Now, there is greater interest in regional climate change by federal, state and local governments. The US Climate Change Science Plan states, "Objective 1.6: Accelerate the development of scientifically based predictive models to provide regional and fine-scale climate and climate-impacts information relevant for scientific research and decision support applications." The California Energy Commission (CEC) has already funded LLNL for developing protocols for intercomparion of regional climate models, and detection of regional climate change. DOE had funded our efforts in high-resolution global modeling through the SciDAC program. Therefore, leadership in global and regional climate modeling demonstrated by this project has the potential to attract funding from CEC and DOE.

The return to the Laboratory of this project is also in the category of *great science*, since we are enhancing an existing leading edge simulation capability that has high international visibility. Our results will be submitted to a leading journal (Journal of Climate) for publication. Our success has led to a higher visibility and a broader collaboration with scientists at National Center for Atmospheric Research, University of Michigan and University of California/Scripps Institution of Oceanography.

7. Summary

We have used a high-resolution configuration of NCAR CCSM3 to perform two stable control simulations. The pre-industrial control simulation is now being used to estimate the natural variability of stream flow in California. This work is done in collaboration with scientists from Scripps Institution of Oceanography. The present-day control simulation is compared to observations and to the well-documented simulation by the standard version of CCSM3 which uses the spectral T85-grid for the atmosphere. There

are major improvements in the simulation of the surface wind stress and sea ice thickness distribution in the Arctic. Surface wind stress and ocean circulation in the Antarctic Circumpolar Current are also improved. Our results demonstrate that the FV version of the CCSM coupled model is a state of the art climate model whose simulation capabilities are in the class of those used for IPCC assessments. The simulated climate is very similar to that of the T85 version in terms of its biases, and more like the T85 model than the other IPCC models. This second part of our work is done in collaboration with scientists from NCAR and University of Michigan. Finally, we have also begun driving a high resolution regional climate model using the boundary conditions from our global model simulations. In this dynamical downscaling procedure, the mesoscale model will be run on climate time scales.

Acknowledgements

This work was performed under the auspices of the U.S. Department of Energy by the University of California Lawrence Livermore National Laboratory under contract No. W-7405-Eng-48. We thank Dr. Lobell for providing the total runoff data in Netcdf data format, and Drs. Ivanova and P. Gleckler for their help in the climate analysis. We also acknowledge the modeling groups for providing their data for analysis, the Program for Climate Model Diagnosis and Intercomparison (PCMDI) for collecting and archiving the model output, and the JSC/CLIVAR Working Group on Coupled Modelling (WGCM) for organizing the model data analysis activity. The multi-model data archive is supported by the Office of Science, U.S. Department of Energy

8. References

Adler, R. F., G. J. Huffman, A. Chang, R. Ferraro, P. P. Xie, J. Janowiak, B. Rudolf, U. Schneider, S. Curtis, D. Bolvin, A. Gruber, J. Susskind, P. Arkin, and E. Nelkin, 2003: The version-2 global precipitation climatology project (GPCP) monthly precipitation analysis (1979-present). *Journal of Hydrometeorology*, **4,** 1147-1167.

Barkstrom, B. R. and G. L. Smith, 1986: The Earth Radiation Budget Experiment - Science and Implementation. *Reviews of Geophysics*, **24,** 379-390.

Bentamy, A., P. Queffeulou, Y. Quilfen, and K. Katsaros, 1999: Ocean surface wind fields estimated from satellite active and passive microwave instruments. *Ieee Transactions on Geoscience and Remote Sensing*, **37,** 2469-2486.

Boville, B. A. and P. R. Gent, 1998: The NCAR Climate System Model, version one. *Journal of Climate*, **11,** 1115-1130.

Briegleb, B. P., C. M. Bitz, E. C. Hunke, W. H. Lipscomb, M. M. Holland, J. L. Schramm, and R. E. Moritz, 2004: Scientific description of the sea ice component of the Community Climate System Model Version Three. Tech. Rep. NCAR/TN-463+STR, National Center for Atmospheric Research, Boulder, CO, 78 pp.

Cavalieri, D. J., P. Gloersen, C. L. Parkinson, J. C. Comiso, and H. J. Zwally, 1997: Observed hemispheric asymmetry in global sea ice changes. *Science*, **278,** 1104-1106.

Collins, W., P. J. Rasch, B. A. Boville, J. J. Hack, J. R. McCaa, D. L. Williamson, J. T. Kiehl, B. P. Briegleb, C. Bitz, S. J. Lin, M. H. Zhang, and Y. Dai, 2006: Description of the NCAR Community Atmosphere Model (CAM 3.0), NCAR Techincal Note, NCAR/TN-464+STR, NCAR, Boulder, CO, USA, 214 pp.

Collins, W. D., P. J. Rasch, B. A. Boville, J. J. Hack, J. R. McCaa, D. L. Williamson, B. P. Briegleb, C. M. Bitz, S. J. Lin, and M. H. Zhang, 2006: The formulation and atmospheric simulation of the Community Atmosphere Model version 3 (CAM3). *Journal of Climate*, **19,** 2144-2161.

Collins, W. D., C. M. Bitz, M. L. Blackmon, G. B. Bonan, C. S. Bretherton, J. A. Carton, P. Chang, S. C. Doney, J. J. Hack, T. B. Henderson, J. T. Kiehl, W. G. Large, D. S. McKenna, B. D. Santer, and R. D. Smith, 2006: The Community Climate System Model version 3 (CCSM3). *Journal of Climate*, **19,** 2122-2143.

DeWeaver, E. and C. M. Bitz, 2006: Atmospheric circulation and its effect on Arctic sea ice in CCSM3 simulations at medium and high resolution. *Journal of Climate*, **19,** 2415-2436..

Hack, J. J., J. M. Caron, G. Danabasoglu, K. W. Oleson, C. Bitz, and J. E. Truesdale, 2006: CCSM-CAM3 climate simulation sensitivity to changes in horizontal resolution. *Journal of Climate*, **19,** 2267-2289.

Harrison, E. F., P. Minnis, B. R. Barkstrom, V. Ramanathan, R. D. Cess, and G. G. Gibson, 1990: Seasonal-Variation of Cloud Radiative Forcing Derived from the Earth Radiation Budget Experiment. *Journal of Geophysical Research-Atmospheres*, **95,** 18687-18703.

Holland, M. M., C. M. Bitz, E. C. Hunke, W. H. Lipscomb, and J. L. Schramm, 2006: Influence of the sea ice thickness distribution on polar climate in CCSM3. *Journal of Climate*, **19,** 2398-2414.

Kalnay, E., M. Kanamitsu, R. Kistler, W. Collins, D. Deaven, L. Gandin, M. Iredell, S. Saha, G. White, J. Woollen, Y. Zhu, M. Chelliah, W. Ebisuzaki, W. Higgins, J. Janowiak, K. C. Mo, C. Ropelewski, J. Wang, A. Leetmaa, R. Reynolds, R. Jenne, and D. Joseph, 1996: The NCEP/NCAR 40-year reanalysis project. *Bulletin of the American Meteorological Society*, **77,** 437-471.

Kiehl, J. T. and K. E. Trenberth, 1997: Earth's annual global mean energy budget. *Bulletin of the American Meteorological Society*, **78,** 197-208.

Kiehl, J. T. and P. R. Gent, 2004: The Community Climate System Model, version 2. *Journal of Climate*, **17,** 3666-3682.

Levitus, S., T. P. Boyer, M. E. Conkright, T. O'Brien, J. Antonov, C. Stephens, L. Stathoplos, D. Johnson, and R. Gelfeld, 1998: World Ocean database 1998, Vol. 1, Introduction, NOAA Atlas NESDIS 18, 346 pp.

Lin, S. J., 1997: A finite-volume integration method for computing pressure gradient force in general vertical coordinates. *Quarterly Journal of the Royal Meteorological Society*, **123,** 1749-1762.

——, 2004: A "vertically Lagrangian" finite-volume dynamical core for global models. *Monthly Weather Review*, **132,** 2293-2307.

Lin, S. J. and R. B. Rood, 1996: Multidimensional flux-form semi-Lagrangian transport schemes. *Monthly Weather Review*, **124,** 2046-2070.

——, 1997: An explicit flux-form semi-Lagrangian shallow-water model on the sphere. *Quarterly Journal of the Royal Meteorological Society*, **123,** 2477-2498.

Queffeulou, P., B. Chapron, and A. Bentamy, 1999: Comparing Ku-band NSCAT scatterometer and ERS-2 altimeter winds. *Ieee Transactions on Geoscience and Remote Sensing*, **37,** 1662-1670.

Randel, D. L., T. H. VonderHaar, M. A. Ringerud, G. L. Stephens, T. J. Greenwald, and C. L. Combs, 1996: A new global water vapor dataset. *Bulletin of the American Meteorological Society*, **77,** 1233-1246.

Rasch, P. J., B. A. Boville, and G. P. Brasseur, 1995: A 3-Dimensional General-Circulation Model with Coupled Chemistry for the Middle Atmosphere. *Journal of Geophysical Research-Atmospheres*, **100,** 9041-9071.

Rasch, P. J., D. B. Coleman, N. Mahowald, D. L. Williamson, S. J. Lin, B. A. Boville, and P. Hess, 2006: Characteristics of atmospheric transport using three numerical formulations for atmospheric dynamics in a single GCM framework. *Journal of Climate*, **19,** 2243-2266.

Rayner, N. A., D. E. Parker, E. B. Horton, C. K. Folland, L. V. Alexander, D. P. Rowell, E. C. Kent, and A. Kaplan, 2003: Global analyses of sea surface temperature, sea ice, and night marine air temperature since the late nineteenth century. *Journal of Geophysical Research-Atmospheres*, **108,** 4407, doi:10.1029/2002JD002670.

——, 2003: Global analyses of sea surface temperature, sea ice, and night marine air temperature since the late nineteenth century. *Journal of Geophysical Research-Atmospheres*, **108,** -.

Rossow, W. B. and R. A. Schiffer, 1999: Advances in understanding clouds from ISCCP. *Bulletin of the American Meteorological Society*, **80,** 2261-2287.

Rothrock, D. A., Y. Yu, and G. A. Maykut, 1999: Thinning of the Arctic sea-ice cover. *Geophysical Research Letters*, **26,** 3469-3472.

Smith, R. D. and P. R. Gent, 2004: Reference manual for the Parallel Ocean Program (POP), ocean component of the Community Climate Model (CCSM2.0 and 3.0). Tech. Rep. LA-UR-02-2484, Los Alamos National Laboratory. [Available online at http://www.ccsm.ucar.edu/models/ccsm3.0/pop.].

Taylor, K. E., 2001: Summarizing multiple aspects of model performance in a single diagram. *Journal of Geophysical Research-Atmospheres*, **106,** 7183-7192.

Uppala, S., P. Kallberg, A. Hernandez, S. Saarenen, M. Fiorino, X. Li, K. Onogi, N. Sokka, U. Andrea, and V. D. C. Bechtold, 2004: ERA 40: ECMWF 45 year reanalysis of the global atmosphere and surface conditions 1957-2002. *ECMWF Newsletter*, **101,** 2-21.

Xie, P. P. and P. A. Arkin, 1997: Global precipitation: A 17-year monthly analysis based on gauge observations, satellite estimates, and numerical model outputs. *Bulletin of the American Meteorological Society*, **78,** 2539-2558.

Yeager, S. G., C. A. Shields, W. G. Large, and J. J. Hack, 2006: The low-resolution CCSM3. *Journal of Climate*, **19,** 2545-2566.

Zhang, Y. C., W. B. Rossow, A. A. Lacis, V. Oinas, and M. I. Mishchenko, 2004: Calculation of radiative fluxes from the surface to top of atmosphere based on ISCCP and other global data sets: Refinements of the radiative transfer model and the input data. *Journal of Geophysical Research-Atmospheres*, **109,** -.

Table 1: Dycore-dependent Parameters for CCSM3 T85 and FVx1 simulations (Collins, W. et al. 2006)

Parameter Description	T85	FVx1
Threshold for autoconversion of warm ice (kg kg^{-1})	4.0e-4	2.0e-4
Threshold for autoconversion of cold ice (kg kg^{-1})	16.0e-6	18.0e-6
Stratiform precipitation evaporation efficiency parameter ((kg m^{-2} s^{-1})$^{-1/2}$ s^{-1})	5.0e-6	5.0e-6
Convective precipitation evaporation efficiency parameter ((kg m^{-2} s^{-1})$^{-1/2}$ s^{-1})	1.0e-6	1.0e-6
Minimum relative humidity threshold for low stable clouds	0.91	0.91
Minimum relative humidity threshold for high stable clouds	0.70	0.77
Parameter for shallow convection cloud fraction	0.07	0.04
Parameter for deep convection cloud fraction	0.14	0.10
Top of area defined to be mid-level cloud (Pa)	250.0e2	750.0e2
Shallow convection precipitation production efficiency parameter (m^{-1})	1.0e-4	1.0e-4
Deep convection precipitation production efficiency parameter (m^{-1})	4.0e-3	3.5e-3

Table 2: Global- and annual-means and root mean square error of selected climate variables

		Mean		RMSE	
Variable	Observation	T85	FVx1	T85	FVx1
Surface air temperature (K)	287.6[a]	287.3	287.4	3.2	3.2
Precipitation (mm/day)	2.6[b]	2.8	2.8	1.4	1.3
Precipitable water (mm)	24.6[c]	23.9	23.9	3.6	3.3
Total cloudiness	66.7[d]	55.8	55.0	15.2	16.4
All-sky outgoing longwave radiation (W m^{-2})	233.9[e]	235.5	235.8	10.9	10.7 10.3
TOA Net all-sky shortwave flux (W m^{-2})	234 .0[e]	237.2	237.5	15.3	18.7 15.3
Longwave cloud forcing (W m^{-2})	30.4[e]	30.3	30.5	9.6	10.1 9.1
Shortwave cloud forcing (W m^{-2})	-54.2 [e]	-54.1	-54.1	17.1	19.4 17.2
Net all-sky surface shortwave (W m^{-2})	165.9[f]	159.5	160.1	17.7	17.7
Net all-sky surface longwave flux (W m^{-2})	49.4[f]	58.4	59.3	15.5	16.1
Latent heat flux (W m^{-2})	84.9[g]	82.8	82.2	21.4	21.4
Sensible heat flux (W m^{-2})	15.8[h]	18.5	18.8	14.5	15.4
Sea level Pressure (mb)	1011.6[h]	1010.6	1011.1	5.0	4.7
200-mb zonal wind (m s^{-1})	15.3[h]	18.4	17.4	4.5	4.0
500-mb geopotential height (m)	5658[h]	5674	5671	36	30

[a]Legates (Legates and Willmott 1990) ; [b]GPCP (Adler et al. 2003); [c]NVAP (Randel et al. 1996); [d]ISSCP (Rossow and Schiffer 1999); [e]ERBE (Barkstrom and Smith 1986;Harrison et al. 1990;Kiehl and Trenberth 1997); [f]ISCCP FD (Zhang et al. 2004); [g]ECMWF (Uppala et al. 2004) ; [h]NCEP (Kalnay et al. 1996)

Fig. 2

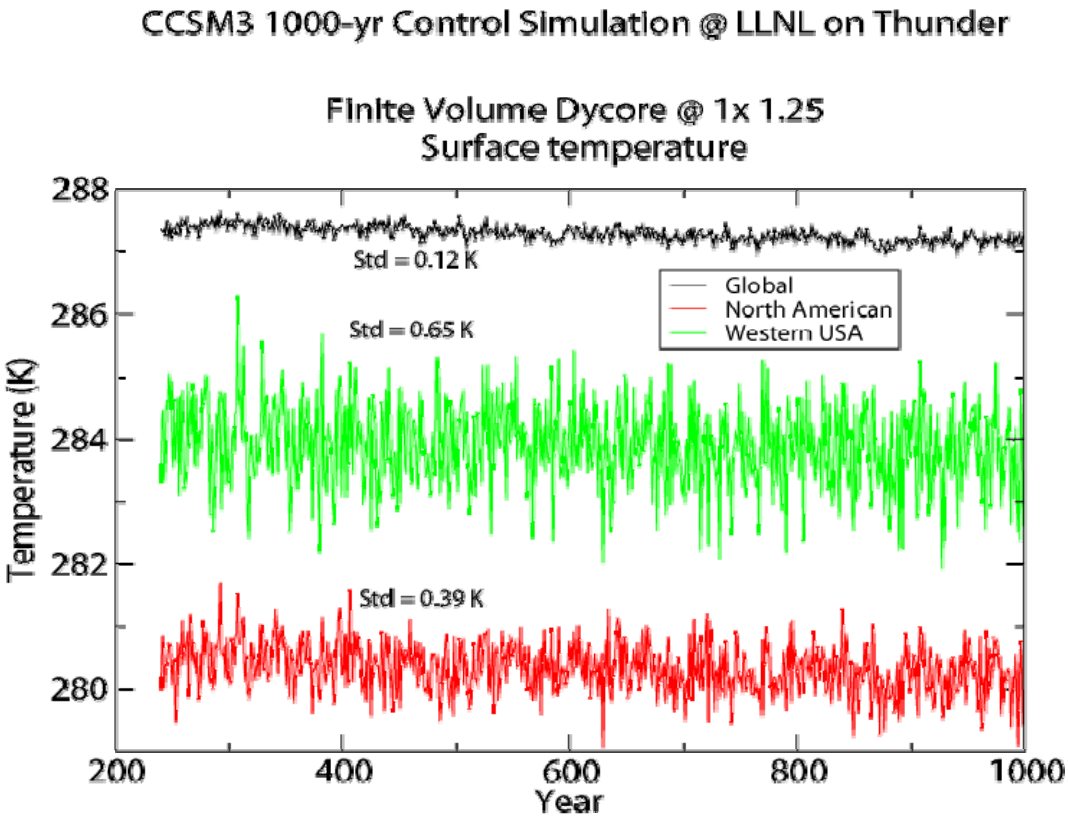

Fig. 2 Time series of annual mean surface temperature over the global (black), North American (red), and the western USA (green) domain. The standard deviation of each time series is also shown.

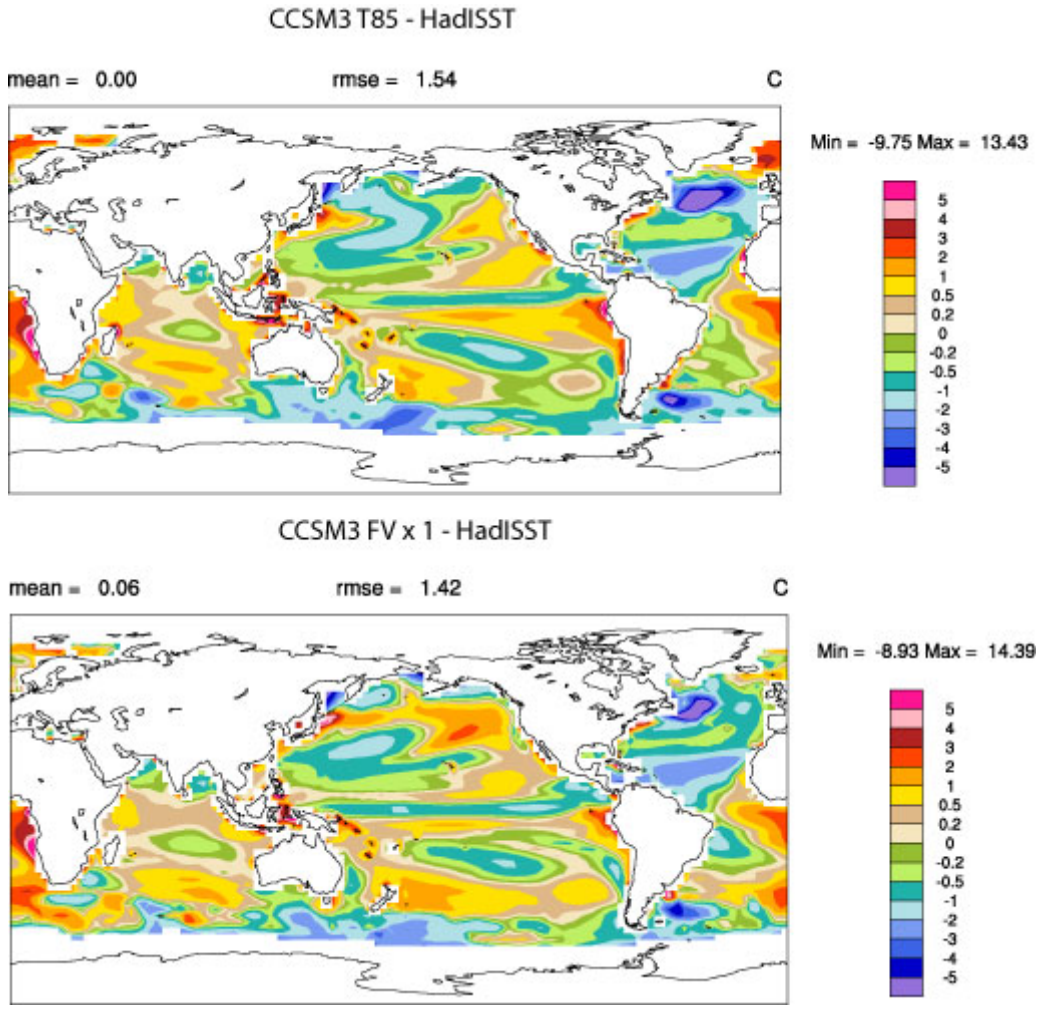

Fig. 3 Differences in annual-mean surface temperature (^{o}C) between CCSM3 (top) T85 simulation and HadISST dataset (Rayner et al. 2003), and (bottom) FVx1 simulation and the HadISST dataset.

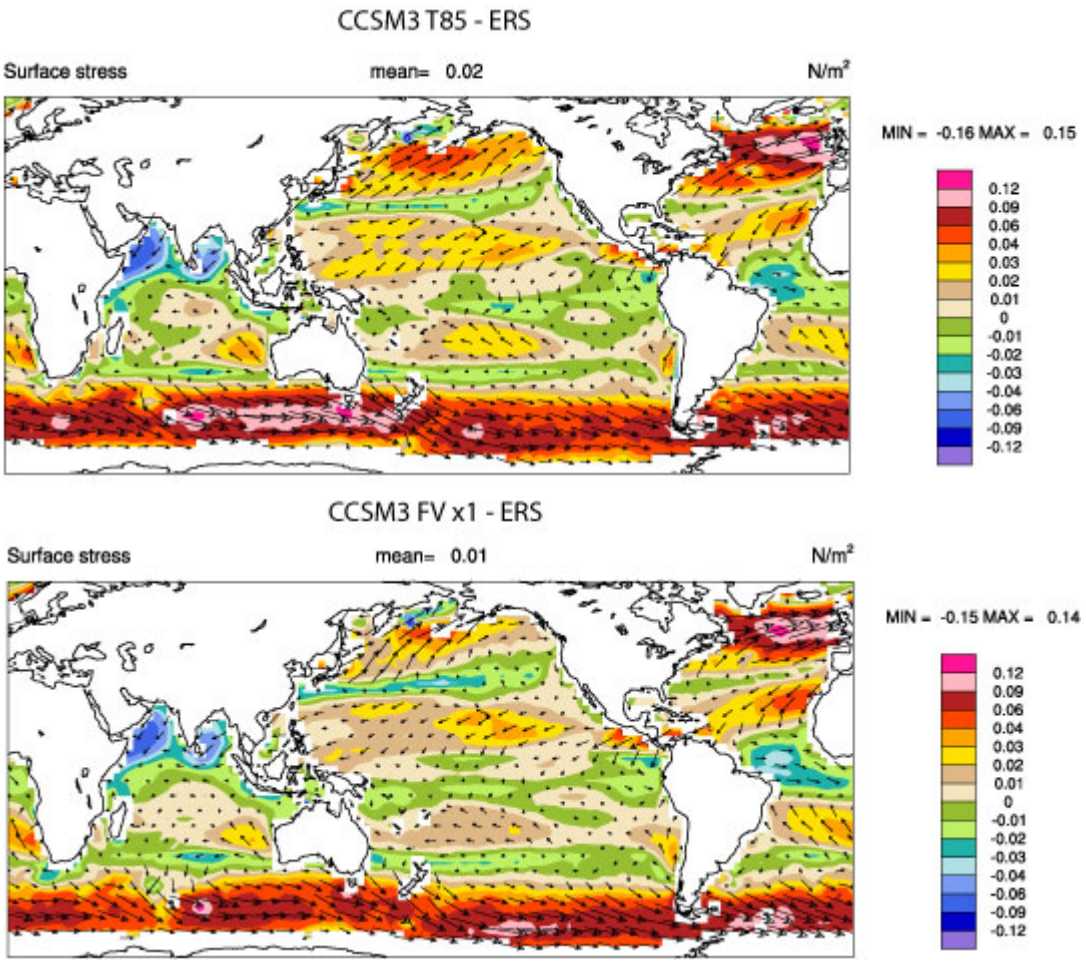

Fig. 4 Differences in annual-mean surface wind stress (Nm^{-2}) between CCSM3 (top) T85 simulation and the ERS dataset (Bentamy et al. 1999), and (bottom) FVx1 simulation and the ERS dataset. The vectors shows the direction of wind stress differences.

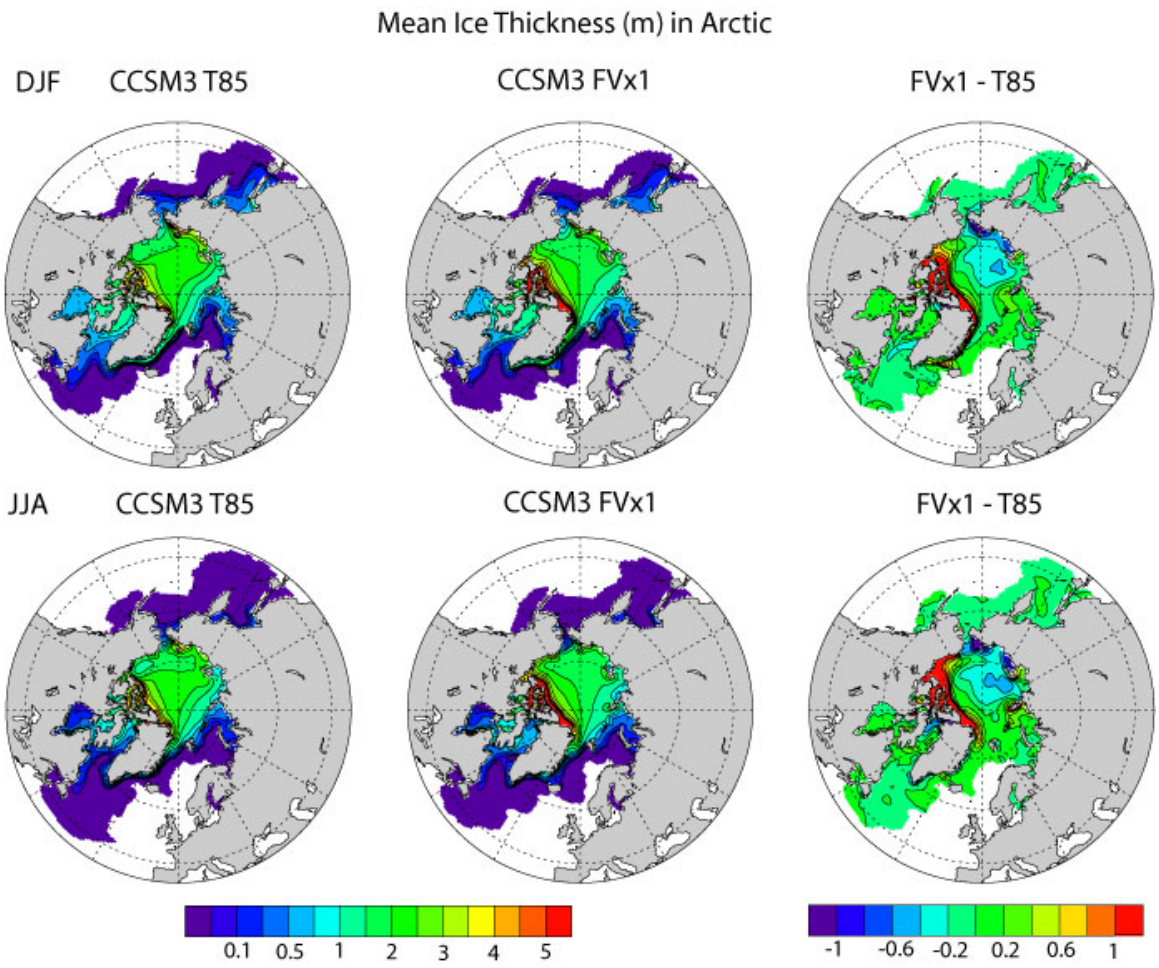

Fig. 5 Mean sea ice thickness (meters) in the Arctic in the Northern Hemisphere (top row) winter and (bottom row) summer in the CCSM3 T85 and FVx1 simulations, and the difference between them.

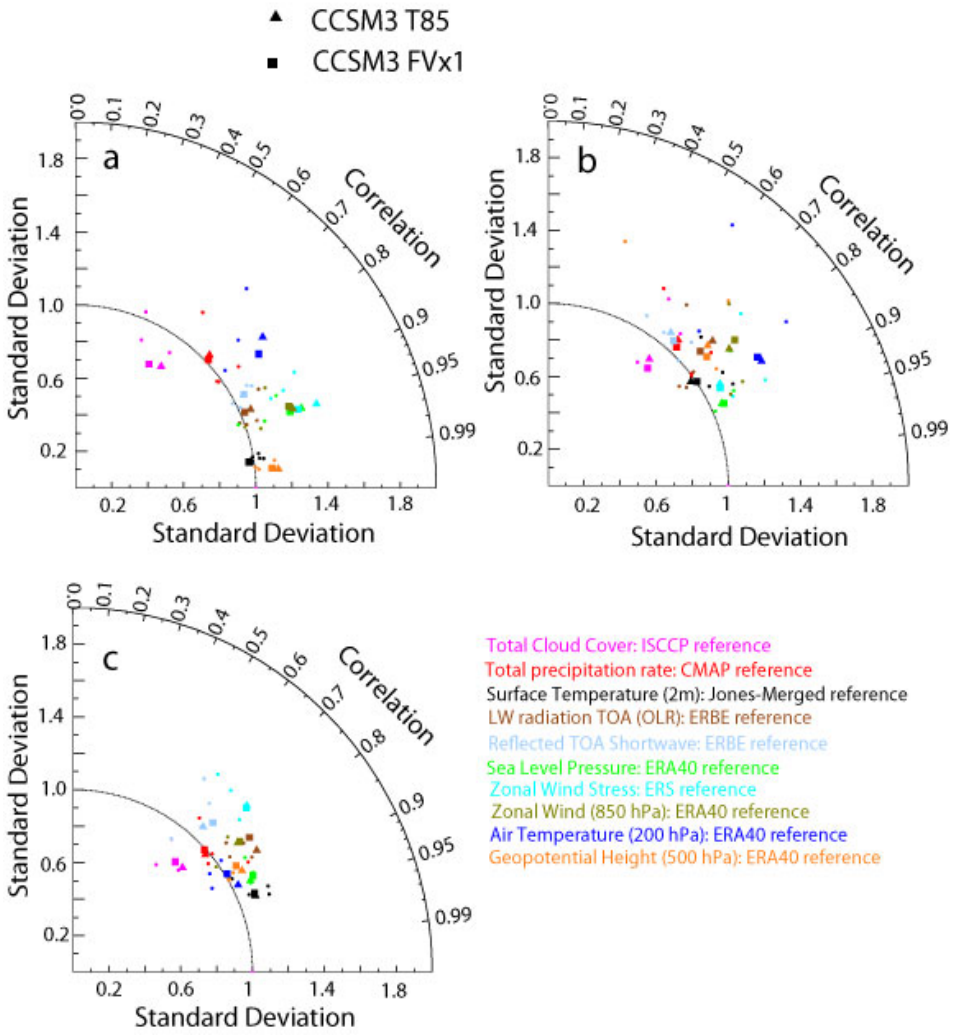

Fig. 6 Taylor diagrams (Taylor 2001) that compare the CCSM3 FVx1 and T85 simulations to a few CMIP3 models. Shown are a) global annual cycle space-time statistics, b) annual cycle space-time statistics for the tropics, and c) annual cycle space-time statistics of zonal-mean anomaly for the Northern Hemisphere extratropics (20^{o}N-90^{o}N). The following reference datasets are used: CMAP (Xie and Arkin 1997) for precipitation, ISCCP (Rossow and Schiffer 1999) for total cloud cover, ERBE (Barkstrom and Smith 1986) for outgoing longwave radiation and reflected shortwave (both at the top of the atmosphere), ERS (Bentamy et al. 1999;Queffeulou et al. 1999) for zonal wind stress (ocean only), an updated version of the Jones 2m temperature dataset (Jones 1988) and ERA40 (Uppala et al. 2004) for winds, temperature, geopotential and sea-level pressure.